Optics Communications 557 (2024) 130343

Contents lists available at ScienceDirect

Optics Communications

journal homepage: www.elsevier.com/locate/optcom

Nonlinear frequency up-conversion of perfect vortex beams based on four wave-mixing in ^{85}Rb atoms

Maolin Zhang, Xuewen Wang, Jinpeng Yuan *, Liantuan Xiao, Suotang Jia, Lirong Wang *

State Key Laboratory of Quantum Optics and Quantum Optics Devices, Institute of Laser Spectroscopy, Shanxi University, 92 Wucheng Road, Taiyuan 030006, China

Collaborative Innovation Center of Extreme Optics, Shanxi University, 92 Wucheng Road, Taiyuan 030006, China

ARTICLE INFO

Keywords:
Orbital angular momentum
Nonlinear frequency up-conversion
Four-wave mixing

ABSTRACT

Optical vortices are widely explored in quantum optics and communication because of their quantized orbital angular momentum, especially its applications in the frequency conversion process lay a foundation for establishing frequency interfaces. However, limited by the spatial mode matching, constructing the frequency interfaces with uniform conversion efficiency is still a challenge. Here, we propose and demonstrate a frequency up-conversion of perfect vortex beams for accommodating arbitrary topological charges in a diamond atomic system of ^{85}Rb. In this process, the 780 nm, 776 nm and internally generated 5233 nm light fields induce the 420 nm coherent blue light generation. The 776 nm perfect vortex beam with transverse structure-invariance serves as the signal beam, which leads to the uniform conversion efficiency and is accompanied by orbital angular momentum transfer of output 420 nm coherent blue light. In addition, in view of the tunable radius and width, the perfect vortex beams with different transverse sizes are also successfully transferred, which further increases the encoding flexibility.

1. Introduction

Structured lights [1] with distinct spatial or spatiotemporal properties [2] are continually advancing the general optics community, such as optical sensing [3,4], optical micromanipulation [5], quantum information processing [6,7], and light-matter interactions [8,9]. As a typical example, the vortex beams [10] carrying orbital angular momentum [11] (OAM) have grown into a significant tool in optical tweezer technology [12,13], high-dimensional quantum entanglement [14–16], and super-resolution imaging [17,18]. On the one hand, the vortex beams are proposed to improve system capacity owing to theoretically infinite topological charges [19]. On the other hand, the propagation stability of phase singularities enables them to develop into robust information carriers, which paves the way for satisfying the requirements of next-generation optical communication [20].

The transfer and manipulation of OAM via nonlinear frequency conversion are widely studied for constructing frequency interfaces of high-dimensional quantum communications [21]. Among various nonlinear media, alkali atoms have become ideal platforms for implementing OAM transfer, storage, and detection due to the high quantum efficiency, abundant energy levels, and low light intensity requirement [22–24]. In previous researches, the phase structure associated with OAM is successfully transferred from near-infrared to blue-violet wavelength through four wave-mixing in Rb atomic vapor [24–27]. The Gouy phase matching and angular momentum conservation dictate the selection rules of the angular mode number in this process, allowing efficient conversion between radial and azimuthal modes [28]. Furthermore, they also have been applied in high-dimensional entanglement protocols and multiplexing, both for classical and quantum communications [29]. However, the nonuniform conversion efficiency remains a challenging task due to the significant dependence of spatial modes, especially for traditional Laguerre-Gaussian beams and Bessel beams [30]. Recently, the concept of perfect vortices, constraining by the Dirac-function [31] and exhibiting transverse structure-invariance for arbitrary topological charges [32], provides a possible solution to overcome the obstacle of intrinsic spatial mode-dependence. Perfect vortex beam (PVB) are typically generated by Fourier transforming Bessel beams, laying the foundation for expanding the applications of vortex beams [33]. This unique property makes them ideal for capturing and manipulating microscopic particles. The spontaneous parametric down-conversion based on PVB has also been experimentally achieved to significantly improve the quality of high-dimensional

* Corresponding authors at: State Key Laboratory of Quantum Optics and Quantum Optics Devices, Institute of Laser Spectroscopy, Shanxi University, 92 Wucheng Road, Taiyuan 030006, China.

E-mail addresses: yjp@sxu.edu.cn (J. Yuan), wlr@sxu.edu.cn (L. Wang).

https://doi.org/10.1016/j.optcom.2024.130343
Received 15 November 2023; Received in revised form 7 January 2024; Accepted 25 January 2024
Available online 30 January 2024

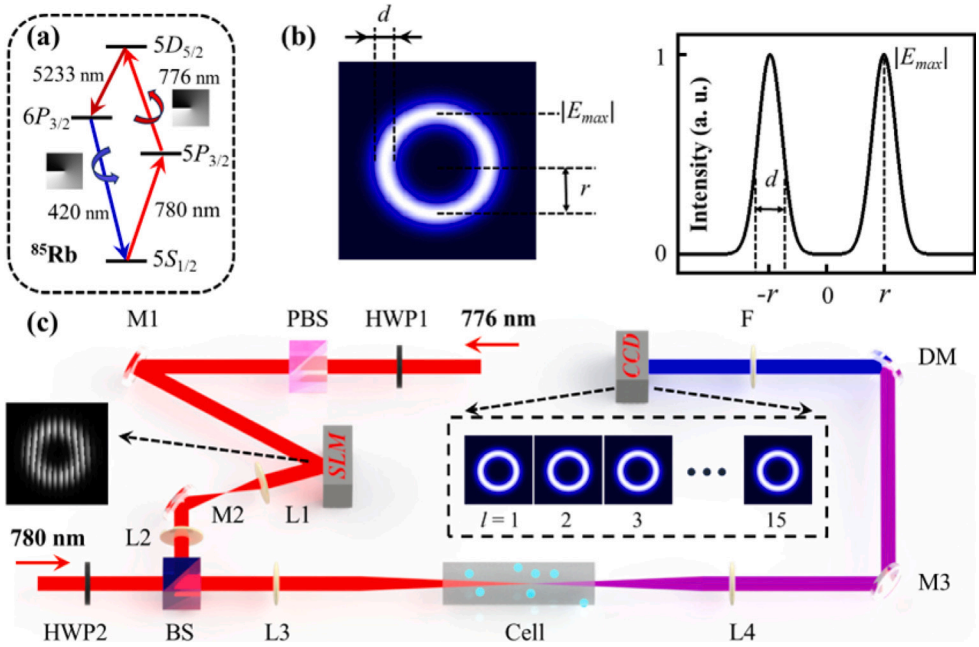

Fig. 1. (a) Relevant energy levels of ^{85}Rb atoms. (b) The diagram of PVB cross-section. (c) Schematic diagram of the experimental setup. HWP: half-wave plate; PBS: polarization beam splitter; M: high reflection mirror; SLM: spatial light modulator; L: Lens; BS: beam splitter; DM: dichroic mirror; F: interference filter; CCD: charge-coupled device.

OAM entangled sources. Therefore, the PVB with a topological charge-independent transverse structure may be one of the best solutions to realize spatial mode matching. Theoretically, after replacing the traditional vortex beam with PVB in nonlinear frequency conversion, the almost same conversion efficiency can be obtained for arbitrary OAM states [34]. However, there is limited research available on this specific process, and more in-depth exploration is still necessary [35].

In this work, we experimentally demonstrate the nonlinear frequency up-conversion of PVB based on four wave-mixing (FWM) in ^{85}Rb atoms [36]. The 776 nm signal beam, combining with 780 nm Gaussian pump and internally generated 5233 nm mid-infrared beams, induces the FWM process, which results in the 420 nm coherent blue light(CBL) generation. Firstly, the transverse structures of incident PVB, represented by radius and width of rings, are compared with conventional Laguerre-Gaussian beam (LGB). The PVB exhibits excellent transverse structure-invariance, and thus effectively overcome the dependence of parametric process on spatial modes to realize the uniform conversion efficiency of 420 nm CBL for arbitrary topological charges *l*. Furthermore, in view of the flexible tunability of PVB, the frequency up-conversion with different combinations of radius and width is studied in detail. The results show that the conversion efficiency is still independent of *l*, which paves the way for establishing continuously tunable frequency interfaces.

2. Experimental setup

Fig. 1(a) shows the relevant energy levels of ^{85}Rb atoms, consisting of $5S_{1/2}$, $5P_{3/2}$, $5D_{5/2}$, and $6P_{3/2}$ states. The 780 nm and 776 nm light fields excite ^{85}Rb atoms from the $5S_{1/2}$ ground state to the $5D_{5/2}$ excited state, inducing the 5233 nm light generation by amplified spontaneous emission. Finally, the 420 nm CBL is generated when the phase matching conditions are met [37,38]. The 780 nm Gaussian beam and 776 nm PVB serve as the pump and signal beam, respectively. Notice, The 5233 nm light field is mainly created by amplified spontaneous emission then $l_{5233} = 0$ is mainly expected. In addition, since the difference in wavelength between the 5233 nm and 420 nm light fields, $l_{5233} = 0$ is the most favorable case to get Rayleigh ranges of the same order of magnitude. Thus, the phase information of 776 nm signal light field is completely transferred to 420 nm output light field. The complex amplitude of a perfect vortex beam E is simplified as [39]:

$$E(r,\varphi) \propto \exp[-(r-r_0)^2/d^2] * \exp(-il\varphi) \quad (1)$$

where (r, φ)s is the polar coordinate, l is the topological charge. The width d is its full width at half maximum, and the radius r_0 is defined as the interval between the propagation axis and the maximum intensity position, as shown in Fig. 1(b).

The schematic diagram of experimental setup is shown in Fig. 1(c). The 780 nm and 776 nm lasers are provided by two tapered amplifier diode lasers (DLC TA pro, Toptica). In order to eliminate the nonlinear lens effect of atomic medium, the frequency detuning is set as $\Delta_{780} = -\Delta_{776} \approx 1.6$ GHz [40,41] corresponded to $5S_{1/2}(F = 3)$–$5P_{3/2}(F' = 4)$–$5D_{5/2}(F'' = 5)$ transitions. The spatial mode of 776 nm signal beam is modulated by complex amplitude modulation technology using a spatial light modulator (SLM, Hamamatsu). In this experiment, the phase hologram generated by complex amplitude modulation (CAM) technique, which simultaneously encodes the amplitude and phase information. The signal light is reflected at a small angle (<15°) and the 1−order diffraction is chosen to obtain PVB described by Eq. (1), while the 780 nm pump beam maintains Gaussian mode. The signal and pump beams with co-propagating configuration enter into a 2 cm long Rb vapor cell, which is housed in a μ-metal to shield stray magnetic field [42]. The temperature is precisely keeping at 130 °C by a self-feedback system, corresponding atomic density is about 3.56×10^{13}cm^{-3}. The powers of pump and signal beams are 60 mW and 10 mW respectively. The generated 420 nm CBL is separated from the background light using a dichroic mirror and an interference filter (center wavelength 420 nm, 10 nm pass band). The charge coupled device (CCD) is employed to record the intensity profiles of the output 420 nm CBL, and the titling lens method [43] is used to detect the topological charge based on astigmatic transformation of vortex beam.

3. Results and discussions

The spatial mode matching [44] is a decisive factor for nonlinear frequency up-conversion, which directly determines the conversion efficiency of output light field. Considering the weak gain regime, the amplitude of output 420 nm CBL $\sqrt{I_B}$ is proportional to $Z\sqrt{I_{776}I_{780}}$,

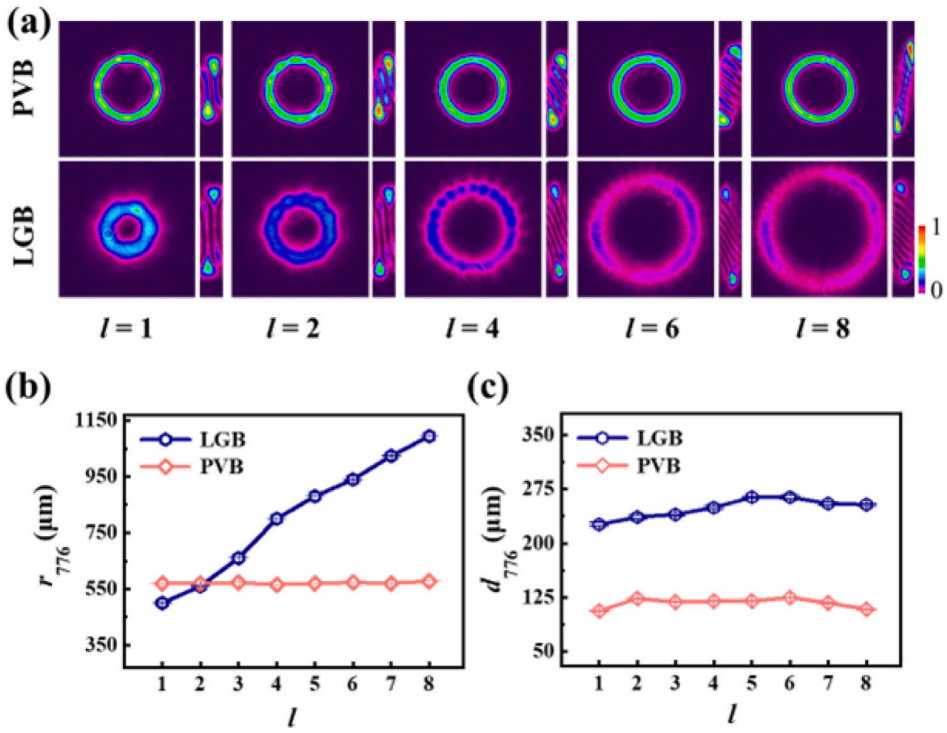

Fig. 2. Comparison of (a) intensity profiles, width and radius for (b) LGB and (c) PVB varying l from 1 to 8. The initial spot radius is almost identical of the incident PVB and LGB, while the widths corresponds to about 120 μm and 260 μm respectively.

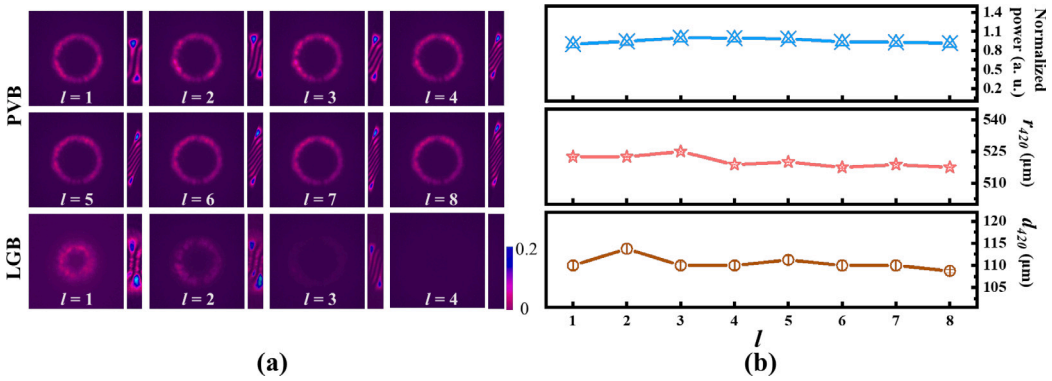

Fig. 3. (a) Intensity profiles of the output 420 nm CBL under the case of incident PVB and LGB respectively. (b) Normalized power, radius, and width of 420 nm CBL for incident PVB. The error represents the standard deviation of three measurements.

where I_{776}, I_{780} represent the intensities of incident fields respectively, and Z is the cell length. Consequently, the conversion efficiency of 420 nm output light field is known to be proportional to the overlap integral of 776 nm signal light field and 780 nm pump light field, which is written as [27]:

$$K_{\ell} = \int_0^{\infty} I_{776}(r) I_{780}(r) 2\pi r dr \tag{2}$$

Obviously, the 776 nm signal light field is constrained by the Dirac function, resulting in l–independent the overlap integral. The uniform conversion efficiency is achieved utilizing PVB to accommodate arbitrary OAM states. Firstly, the transverse structure of 776 nm PVB is compared with the case of traditional LGB in detail, which is characterized by the width d_{776} and radius r_{776} of rings. Fig. 2(a) shows the intensity profile of PVB and LGB with different l. It can be intuitively seen that the transverse size of PVB remains almost constant, while LGB changes with increasing l. The topological charge l of the signal beam is detected using a tilted lens and displayed on the right side of the intensity profile. The number of the dark stripes is equal to the number of topological charges. To analyze the difference quantitatively, the corresponding d_{776} and r_{776} of LGB and PVB are measured by taking the average intensity profile along the azimuthal angle, as shown in Fig. 2(b) and (c). It can be seen that the width and radius of PVB are almost stable at ~120 and ~550 μm respectively when the topological charge is changed from l = 1 to 8. Conversely, although the width of LGB remains 240 μm, the radius increases about from 500 μm for l = 1 to 1070 μm for l = 8. Therefore, in compared to the LGB, the PVB exhibits greater compatibility for arbitrary topological charges in nonlinear frequency up-conversion.

In order to further explore the influence of PVB and LGB on frequency up-conversion, Fig. 3(a) shows the intensity profiles of output 420 nm CBL under these two cases. The powers of the signal and pump beams are set at 10 mW and 60 mW, respectively. In addition, we choose the appropriate widths of the beams to improve the nonlinear interaction [45]. As expected, the output 420 nm CBL under the case of PVB has consistent conversion efficiency, perfectly inheriting the characteristics of the incident PVB. However, when LGB is used as signal beam, the spatial mode mismatching results in decreasing the

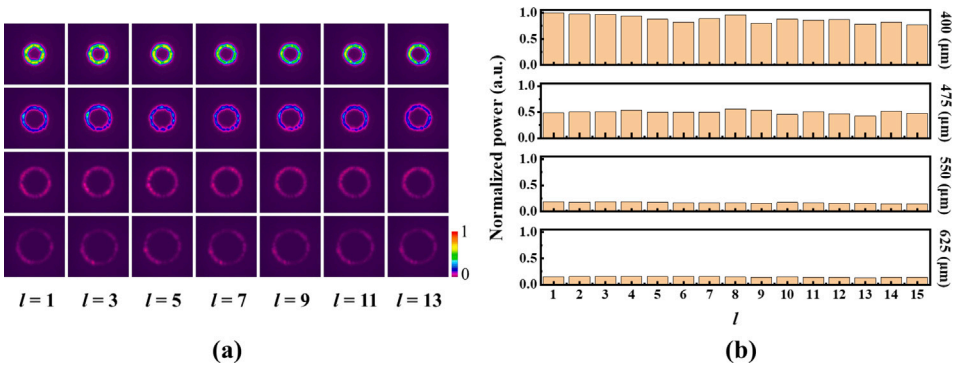

Fig. 4. (a) Intensity profiles and (b) normalized power of the output 420 nm CBL with different r_{776}. The width is fixed at 120 μm, and the initial radius from top to bottom corresponds to 400 μm, 475 μm, 550 μm, and 625 μm respectively.

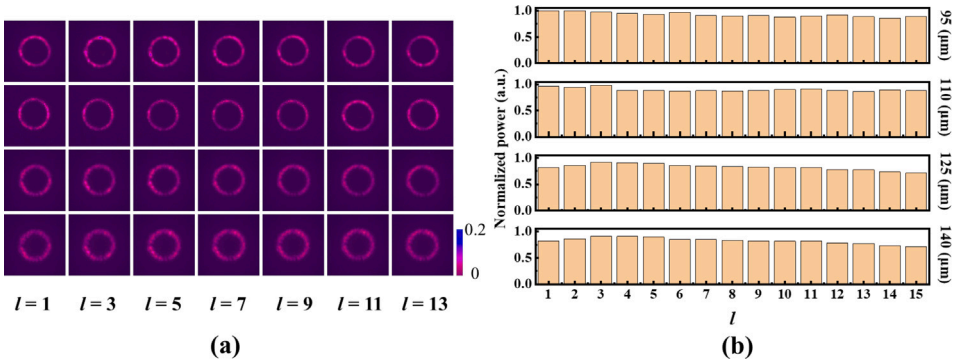

Fig. 5. (a) Intensity profiles and (b) normalized power of the output 420 nm CBL with different d_{776}. The radius is fixed at 550 μm, and the initial width from top to bottom corresponds to 95 μm, 110 μm, 125 μm, and 140 μm respectively.

gain of the FWM process with increasing the l. Thus, the frequency up-conversion of LGB of only $l = 1$ to 4 can be achieved in the existing system. Furthermore, the normalized power, radius and width of output 420 nm PVB are quantitatively analyzed, as shown in Fig. 3(b). Obviously, the conversion efficiency remains stable as increasing l from 1 to 8, which can be continually increased in theory. And the radius and width of ring are maintained at about 524 μm and 113 μm respectively. The above results indicate that the PVB can effectively overcome the dependence of spatial modes to realize the uniform conversion efficiency compared with the traditional LGB, which hold tremendous prospect for establishing frequency interfaces with continuously tunable topological charges. It is worth noting that this system is also applicable for the case of negative topological charges.

In addition to the l-independent transverse structures, another advantage of the PVB is the precisely and flexibly tunable radius and width. Furthermore, a detailed investigation is conducted on the impact of radius and width on the conversion efficiency. Fig. 4(a) shows the intensity profiles of output 420 nm CBL by setting the r_{776} of about 400 μm, 475 μm, 550 μm, and 625 μm respectively, corresponding to the first to fourth rows. Here, the width is fixed at 120 μm, and other experimental parameters are consistent with the Fig. 3. The fitted radius of output 420 nm CBL are about 389 μm, 461 μm, 524 μm, 605 μm. Although there are slight differences between the signal and output beams, the conversion efficiency and lateral structure of CBL is immune to topological charge l. Then, the output power normalized to the case of $r_{776} = 400$ μm and $l = 1$ is shown in Fig. 4(b), which also exhibits nearly consistent conversion efficiency for arbitrary topological charges. However, the conversion efficiency reduces with the increased radius, which is because that the signal beam is overlapped with the lower intensity portion of Gaussian pump beam.

The output 420 nm CBL is determined by the mode overlap integral, thus we speculate that the influence of the PVB width is similar to radius, which also does not change as l increases. Next, Fig. 5(a) and (b) show the intensity profiles and normalized power of the output 420 nm CBL with the widths of about 95 μm, 110 μm, 125 μm, and 140 μm (first to forth rows) when the radius is fixed at about 550 μm. Correspondingly, the widths of output 420 nm CBL are about 88 μm, 104 μm, 113 μm, and 125 μm, respectively, and the conversion efficiency is nearly unchanged with topological charges. Above results confirm that the stable frequency up-conversion is realized by utilizing the PVB due to l-independent modal overlap integral under the fixed beam sizes. The defect of conventional LGB not only loses the flexibility of manipulation, but also limits the application of OAM, while the flexible and precise tunability of PVB dramatically increase encoding potential in frequency up-conversion and facilitatly realize a faithful transform of different OAM states.

4. Conclusion

In summary, we demonstrate a frequency up-conversion with uniform conversion efficiency based on perfect vortex beams for accommodating arbitrary topological charges in a diamond atomic system of ^{85}Rb. Firstly, the conventional LGB and PVB are intuitively compared during the frequency up-conversion process. Different from LGBs, the incident PVB with transverse structure-invariance efficiently overcome the spatial amplitude dependence of the parametric interaction. The output 420 nm CBL perfectly inherits the characteristics of the 776 nm PVB, including spatial amplitude and wavefront phase. Particularly, in view of the tunable radius and width, the PVB with different transverse sizes are also successfully transferred. Our work has expanded considerably the encoding flexibility of information, which is promising for high-dimensional quantum information networks and long-distance quantum communication.

CRediT authorship contribution statement

Maolin Zhang: Conceptualization, Data curation, Formal analysis, Methodology, Writing – original draft, Writing – review & editing. **Xuewen Wang:** Conceptualization, Writing – original draft, Writing – review & editing. **Jinpeng Yuan:** Conceptualization, Methodology, Resources. **Liantuan Xiao:** Conceptualization, Funding acquisition. **Suotang Jia:** Conceptualization, Resources. **Lirong Wang:** Conceptualization, Methodology, Resources.

Declaration of competing interest

The authors declare that they have no known competing financial interests or personal relationships that could have appeared to influence the work reported in this paper.

Data availability

Data will be made available on request.

Acknowledgments

This work was supported in part by the NSFC, China under Grant 62075121; in part by the Fund Program for the Scientific Activities of Selected Returned Overseas Professionals in Shanxi Province, China under Grant 2023001; in part by the Fund for Shanxi "1331 Project", China; and in part by the Fund for Postdoctoral Fellowship Program of CPSF, China under Grant GZC20231510.

References

[1] A. Forbes, M. de Oliveira, M.R. Dennis, Structured light, Nat. Photonics 15 (4) (2021) 253–262, http://dx.doi.org/10.1038/s41566-021-00780-4.
[2] C. He, Y. Shen, A. Forbes, Towards higher-dimensional structured light, Light: Sci. Appl. 11 (1) (2022) http://dx.doi.org/10.1038/s41377-022-00897-3.
[3] S. Murali, N. Quarles, L.L. Zhang, J.R. Potts, Z. Tan, Y. Lu, Y. Zhu, R.S. Ruoff, Volumetric capacitance of compressed activated microwave-expanded graphite oxide (a-MEGO) electrodes, Nano Energy 2 (5) (2013) 764–768, http://dx.doi.org/10.1016/j.nanoen.2013.01.007.
[4] L. Fang, M.J. Padgett, J. Wang, Sharing a common origin between the rotational and linear Doppler effects, Laser Photonics Rev. 11 (6) (2017) http://dx.doi.org/10.1002/lpor.201700183.
[5] M. Padgett, R. Bowman, Tweezers with a twist, Nat. Photonics 5 (6) (2011) 343–348, http://dx.doi.org/10.1038/nphoton.2011.81.
[6] Y. Zhang, M. Agnew, T. Roger, F.S. Roux, T. Konrad, D. Faccio, J. Leach, A. Forbes, Simultaneous entanglement swapping of multiple orbital angular momentum states of light, Nature Commun. 8 (1) (2017) http://dx.doi.org/10.1038/s41467-017-00706-1.
[7] J. Liu, I. Nape, Q. Wang, A. Vallés, J. Wang, A. Forbes, Multidimensional entanglement transport through single-mode fiber, Sci. Adv. 6 (4) (2020) http://dx.doi.org/10.1126/sciadv.aay0837.
[8] D. Ayuso, O. Neufeld, A.F. Ordonez, P. Decleva, G. Lerner, O. Cohen, M. Ivanov, O. Smirnova, Synthetic chiral light for efficient control of chiral light–matter interaction, Nat. Photonics 13 (12) (2019) 866–871, http://dx.doi.org/10.1038/s41566-019-0531-2.
[9] J. Wang, F. Castellucci, S. Franke-Arnold, Vectorial light–matter interaction: Exploring spatially structured complex light fields, AVS Quantum Sci. 2 (3) (2020) http://dx.doi.org/10.1116/5.0016007.
[10] P. Coullet, L. Gil, F. Rocca, Optical vortices, Opt. Commun. 73 (5) (1989) 403–408, http://dx.doi.org/10.1016/0030-4018(89)90180-6.
[11] L. Allen, M.W. Beijersbergen, R.J.C. Spreeuw, J.P. Woerdman, Orbital angular momentum of light and the transformation of Laguerre-Gaussian laser modes, Phys. Rev. A 45 (11) (1992) 8185–8189, http://dx.doi.org/10.1103/physreva.45.8185.
[12] Y. Yan, J. Yuan, L. Wang, L. Xiao, S. Jia, A dual-wavelength bandpass faraday anomalous dispersion optical filter operating on the D1 and D2 lines of rubidium, Opt. Commun. 509 (2022) 127855, http://dx.doi.org/10.1016/j.optcom.2021.127855.
[13] C. Lóxpez-Mariscal, J.C. Gutiérrez-Vega, G. Milne, K. Dholakia, Orbital angular momentum transfer in helical Mathieu beams, Opt. Express 14 (9) (2006) 4182, http://dx.doi.org/10.1364/oe.14.004182.
[14] A. Mair, A. Vaziri, G. Weihs, A. Zeilinger, Entanglement of the orbital angular momentum states of photons, Nature 412 (6844) (2001) 313–316, http://dx.doi.org/10.1038/35085529.
[15] M. Mafu, A. Dudley, S. Goyal, D. Giovannini, M. McLaren, M.J. Padgett, T. Konrad, F. Petruccione, N. Lütkenhaus, A. Forbes, Higher-dimensional orbital-angular-momentum-based quantum key distribution with mutually unbiased bases, Phys. Rev. A 88 (3) (2013) 032305, http://dx.doi.org/10.1103/physreva.88.032305.
[16] Q. Hu, X. Wang, R. Zhang, Y. Ren, S. Liu, J. Jing, Enhancing and flattening multiplexed quantum entanglement by utilizing perfect vortex modes, Opt. Lett. 48 (7) (2023) 1782, http://dx.doi.org/10.1364/ol.482249.
[17] Y. Kozawa, D. Matsunaga, S. Sato, Superresolution imaging via superoscillation focusing of a radially polarized beam, Optica 5 (2) (2018) 86, http://dx.doi.org/10.1364/optica.5.000086.
[18] M. Yoshida, Y. Kozawa, S. Sato, Subtraction imaging by the combination of higher-order vector beams for enhanced spatial resolution, Opt. Lett. 44 (4) (2019) 883, http://dx.doi.org/10.1364/ol.44.000883.
[19] J. Yuan, H. Zhang, C. Wu, G. Chen, L. Wang, L. Xiao, S. Jia, Creation and control of vortex-beam arrays in atomic vapor, Laser Photonics Rev. 17 (5) (2023) http://dx.doi.org/10.1002/lpor.202200667.
[20] J. Wang, Y. Liang, Generation and detection of structured light: A review, Front. Phys. 9 (2021) http://dx.doi.org/10.3389/fphy.2021.688284.
[21] X. Qiu, H. Guo, Y. Ren, L. Chen, High-dimensional photonic orbital-angular-momentum frequency interface, Phys. Rev. A 19 (4) (2023) 044072, http://dx.doi.org/10.1103/physrevapplied.19.044072.
[22] J. Yuan, T. Jin, L. Xiao, S. Jia, L. Wang, A rydberg atom-based receiver with amplitude modulation technique for the fifth-generation millimeter-wave wireless communication, IEEE Antennas Wirel. Propag. Lett. 22 (10) (2023) 2580–2584, http://dx.doi.org/10.1109/LAWP.2023.3297729.
[23] T. Jin, S. Li, J. Yuan, L. Wang, L. Xiao, S. Jia, Coherent population transfer of Rydberg atoms in a dual-microwave driven five-level configuration, Opt. Commun. 522 (2022) 128603, http://dx.doi.org/10.1016/j.optcom.2022.128603.
[24] N. Liu, X. Wang, J. Yuan, L. Xiao, S. Jia, L. Wang, Manipulation of the orbital angular momentum via four-wave mixing in Rb vapor, Laser Phys. Lett. 20 (3) (2023) 035204, http://dx.doi.org/10.1088/1612-202x/acb43d.
[25] G. Walker, A.S. Arnold, S. Franke-Arnold, Trans-spectral orbital angular momentum transfer via four-wave mixing in rb vapor, Phys. Rev. Lett. 108 (24) (2012) 243601, http://dx.doi.org/10.1103/physrevlett.108.243601.
[26] A.M. Akulshin, I. Novikova, E.E. Mikhailov, S.A. Suslov, R.J. McLean, Arithmetic with optical topological charges in stepwise-excited Rb vapor, Opt. Lett. 41 (6) (2016) 1146, http://dx.doi.org/10.1364/ol.41.001146.
[27] A. Chopinaud, M. Jacquey, B.V. de Lesegno, L. Pruvost, High helicity vortex conversion in a rubidium vapor, Phys. Rev. A 97 (6) (2018) 063806, http://dx.doi.org/10.1103/physreva.97.063806.
[28] R.F. Offer, A. Daffurn, E. Riis, P.F. Griffin, A.S. Arnold, S. Franke-Arnold, Gouy phase-matched angular and radial mode conversion in four-wave mixing, Phys. Rev. A 103 (2) (2021) l021502, http://dx.doi.org/10.1103/physreva.103.l021502.
[29] Y. Zhou, M. Mirhosseini, S. Oliver, J. Zhao, S.M.H. Rafsanjani, M.P.J. Lavery, A.E. Willner, R.W. Boyd, Using all transverse degrees of freedom in quantum communications based on a generic mode sorter, Opt. Express 27 (7) (2019) 10383, http://dx.doi.org/10.1364/oe.27.010383.
[30] X. Wang, J. Yuan, L. Wang, L. Xiao, S. Jia, Enhanced frequency up-conversion based on four-wave mixing assisted by a Bessel-Gaussian beam in 85Rb atoms, Opt. Laser Technol. 149 (2022) 107874, http://dx.doi.org/10.1016/j.optlastec.2022.107874.
[31] Z.-F. Liu, Z.-C. Ren, Y.-C. Lou, Z.-M. Cheng, Y.-X. Yang, Y. Li, J. Ding, X.-L. Wang, H.-T. Wang, Control of harmonic orbital angular momentum in second-harmonic generation of perfect vortices, Phys. Rev. A 105 (6) (2022) 063518, http://dx.doi.org/10.1103/physreva.105.063518.
[32] I. Nape, K. Singh, A. Klug, W. Buono, C. Rosales-Guzman, A. McWilliam, S. Franke-Arnold, A. Kritzinger, P. Forbes, A. Dudley, A. Forbes, Revealing the invariance of vectorial structured light in complex media, Nat. Photonics 16 (7) (2022) 538–546, http://dx.doi.org/10.1038/s41566-022-01023-w.
[33] W. Zhang, Y. Ye, L. Zeng, E. Li, J. Peng, D. Ding, B. Shi, High-dimensional frequency conversion in a hot atomic system, Chin. Opt. Lett. 21 (9) (2023) 092701, http://dx.doi.org/10.3788/col202321.092701.
[34] L. Zeng, Y.-H. Ye, M.-X. Dong, W.-H. Zhang, E.-Z. Li, D.-C. Li, D.-S. Ding, B.-S. Shi, Optical memory for arbitrary perfect Poincaré states in an atomic ensemble, Opt. Lett. 48 (2) (2023) 477, http://dx.doi.org/10.1364/ol.479915.
[35] Y. Shen, X. Wang, Z. Xie, C. Min, X. Fu, Q. Liu, M. Gong, X. Yuan, Optical vortices 30 years on: OAM manipulation from topological charge to multiple singularities, Light: Sci. Appl. 8 (1) (2019) http://dx.doi.org/10.1038/s41377-019-0194-2.
[36] A. Vernier, S. Franke-Arnold, E. Riis, A.S. Arnold, Enhanced frequency up-conversion in Rb vapor, Opt. Express 18 (16) (2010) 17020, http://dx.doi.org/10.1364/oe.18.017020.
[37] F. Kong, C. Zhang, F. Bouchard, Z. Li, G.G. Brown, D.H. Ko, T.J. Hammond, L. Arissian, R.W. Boyd, E. Karimi, P.B. Corkum, Controlling the orbital angular momentum of high harmonic vortices, Nature Commun. 8 (1) (2017) http://dx.doi.org/10.1038/ncomms14970.

[38] G. Gariepy, J. Leach, K.T. Kim, T.J. Hammond, E. Frumker, R.W. Boyd, P.B. Corkum, Creating high-harmonic beams with controlled orbital angular momentum, Phys. Rev. Lett. 113 (15) (2014) 153901, http://dx.doi.org/10.1103/physrevlett.113.153901.

[39] F. Zhu, S. Huang, W. Shao, J. Zhang, M. Chen, W. Zhang, J. Zeng, Free-space optical communication link using perfect vortex beams carrying orbital angular momentum (OAM), Opt. Commun. 396 (2017) 50–57, http://dx.doi.org/10.1016/j.optcom.2017.03.023.

[40] A.M. Akulshin, R.J. McLean, A.I. Sidorov, P. Hannaford, Coherent and collimated blue light generated by four-wave mixing in Rb vapour, Opt. Express 17 (25) (2009) 22861, http://dx.doi.org/10.1364/oe.17.022861.

[41] J.F. Sell, M.A. Gearba, B.D. DePaola, R.J. Knize, Collimated blue and infrared beams generated by two-photon excitation in Rb vapor, Opt. Lett. 39 (3) (2014) 528, http://dx.doi.org/10.1364/ol.39.000528.

[42] S.-D. Wang, J.-P. Yuan, L.-R. Wang, L.-T. Xiao, S.-T. Jia, Investigation on the Cs $6S_{1/2}$ to 7D electric quadrupole transition via monochromatic two-photon process at 767 nm, Front. Phys. 16 (1) (2020) http://dx.doi.org/10.1007/s11467-020-0988-y.

[43] P. Vaity, J. Banerji, R. Singh, Measuring the topological charge of an optical vortex by using a tilted convex lens, Phys. Lett. A 377 (15) (2013) 1154–1156, http://dx.doi.org/10.1016/j.physleta.2013.02.030.

[44] Y. Chen, R. Ni, Y. Wu, L. Du, X. Hu, D. Wei, Y. Zhang, S. Zhu, Phase-matching controlled orbital angular momentum conversion in periodically poled crystals, Phys. Rev. Lett. 125 (14) (2020) 143901, http://dx.doi.org/10.1103/physrevlett.125.143901.

[45] R.N. Lanning, Z. Xiao, M. Zhang, I. Novikova, E.E. Mikhailov, J.P. Dowling, Gaussian-beam-propagation theory for nonlinear optics involving an analytical treatment of orbital-angular-momentum transfer, Phys. Rev. A 96 (1) (2017) 013830, http://dx.doi.org/10.1103/physreva.96.013830.